



## Data worth analysis within a model-free data assimilation framework for soil moisture flow

Yakun Wang<sup>1</sup>, Xiaolong Hu<sup>2</sup>, Lijun Wang<sup>2</sup>, Jinmin Li<sup>2</sup>, Lin Lin<sup>2</sup>, Kai Huang<sup>3</sup>,  
Liangsheng Shi<sup>2\*</sup>

5 <sup>1</sup>Key Laboratory of Agricultural Soil and Water Engineering of in Arid and Semiarid Areas, Ministry of Education, Northwest A & F University, Yangling, Shaanxi 712100, China

<sup>2</sup>State Key Laboratory of Water Resources and Hydropower Engineering Sciences, Wuhan University, Wuhan, Hubei 430072, China

10 <sup>3</sup>Guangxi Key Laboratory of Water Engineering Materials and Structures, Guangxi Institute of Water Resources Research, Nanning530023, China

*Correspondence to:* Liangsheng Shi (liangshs@whu.edu.cn)

**Abstract.** Conventional data-worth (DW) analysis for soil water problems depends on physical dynamic models. The widespread occurrence of model structural errors and the strong nonlinearity of soil water flow may lead to biased or wrong worth assessment. By introducing the nonparametric data-worth analysis (NP-DWA) framework coupled with ensemble Kalman filter (EnKF), this real-world case study attempts to assess the worth of potential soil moisture observations regarding the reconstruction of fully data-driven soil water flow models prior to data gathering. The DW of real-time soil moisture observations after Gaussian process training and Kalman update was quantified with three representative information metrics, including the trace, Shannon entropy difference, and relative entropy. The sequential NP-DWA framework was examined by a number of cases in terms of the variable of interest, spatial location, observation error, and prior data content. Our results indicated that the overall increasing trend of the DW from the sequential augmentation of additional observations was susceptible to interruptions by localized surges due to never-experienced atmospheric conditions (i.e., rainfall events) within the NP-DWA framework. Fortunately, this performance degradation can be effectively alleviated by enriching training scenarios or the appropriate amplification of observational noise under extreme meteorological conditions. Nevertheless, a substantial expansion of the prior data content may cause an unexpected increase in DW of future potential observations due to the possible introduction of ensuing observation noises. Hence, high-quality and representative “small” data may be a better choice than unfiltered “big” data. Compared with the observations in the surface layer with the strongest time-variability, the soil water content in the middle layer robustly exhibited remarkable

15  
20  
25  
30



35 superiority in the construction of model-free soil moisture models. An alternative monitoring strategy with a larger data-worth was prone to a higher DW assessment accuracy within the proposed NP-DWA framework. We also demonstrated that the DW assessment performance was jointly determined by ‘3C’, i.e., capacity of potential observation realizations to “capture” actual observations, correlation of potential observations with the variables of interest, and choice of DW indicators. Direct mapping from regular meteorological data to soil water content within the NP-DWA mitigated the adverse effects of nonlinearity-related interference, which thus facilitated the identification of the soil moisture covariance matrix, especially the cross-covariance.

**Keywords:** Data worth; Nonparametric data assimilation; Soil moisture; Gaussian process

40

## 1 Introduction

As one of the few directly observable hydrological variables, soil water content (SWC) exhibits critical importance in optimal water resource management, irrigation and drainage schemes, fertilizer application, and crop production in agriculture (Liu et al., 2011; Akhtar et al., 2019; Dobriyal et al., 45 2012; Gu et al., 2021). Various data assimilation (DA) approaches (Dunne and Entekhabi, 2005; Li and Ren, 2011; Reichle et al., 2008; Song et al., 2014) have been established to reconstruct the spatiotemporal dynamics of SWC from noisy or partial observations. The core of these traditional parametric filters is their reliance on repeated forward integrations of an explicitly known physical model of unsaturated flow, such as the HYDRUS (Šimůnek et al., 2006), Soil and Water Assessment 50 Tool (SWAT) (Van Dam and Feddes, 2000), and Ross models (Ross, 2003; Zha et al., 2013).

Currently, the ever-increasing availability of multi-source data from remote sensing (Montzka et al., 2011; Shi et al., 2011), ground-based measurements (Li et al., 2018; Shuwen et al., 2005; Yang et al., 2000), and numerical modeling has paved the way for the development of fully data-driven techniques within the DA framework. In particular, recent advances in machine learning-based DA schemes 55 (Brajard et al., 2020; Brajard et al., 2021; Yamanaka et al., 2019) offer exciting new opportunities for extracting patterns and insights of soil moisture dynamics from data (Ju et al., 2018; Li et al., 2020; Liu et al., 2020; Wang et al., 2021a). For instance, Kashif Gill et al. (2007) proposed a hybrid DA methodology that combined support vector machines and the ensemble Kalman filter (EnKF) for soil moisture dynamics. Li et al. (2020) compared the performance of a physical-based model with DA and 60 machine learning methods in terms of the simulation of soil water dynamics under synthetic and



real-world conditions. Wang et al. (2021a) and Wang et al. (2021b) further attempted to learn unknown relationships between SWC as well as its spatio-temporal gradients and highly accessible data via the Gaussian process (GP) regression.

65 Notwithstanding the success of these model-free DA schemes built on machine learning for unsaturated flow, essential caveats and limitations have hampered their further adoption and impact. First, the amount of data required to infer nonlinear relationships in unsaturated flow problems may be overwhelming (Hughes, 1968), thus greatly increasing the data collection budget. Subsequently, addressing the abovementioned explosive data growth is also a challenging and time-demanding task requiring an extensive computational infrastructure. Second, the performance and quality of the  
70 knowledge extracted by machine learning algorithms are highly dependent on the quality and suitability of data (García-Gil et al., 2019). Unfortunately, data gathering is rarely perfect, and data corruption often occurs (Wang et al., 2018). The identification of the multi-source SWC data quality or measurement error is not an easy task. This limitation instead can create extra uncertainties in DA systems (Kisekka et al., 2015). Third, it is the diversity of scenarios contained in prior data rather than  
75 its volume that is more decisive for the generalization ability of machine learning methods (Wang et al., 2020). Direct data fusion without screening may instead induce accidental correlations in learning algorithms, thereby diminishing their generalization ability (García et al., 2016). To avoid the overloaded monitoring cost due to redundant data, it is essential to develop a framework to assess the worth of alternative sampling strategies prior to data collection.

80 Data worth, sometimes called data information content or data impact, of a design is often defined as its individual capability to reduce uncertainty associated with a prediction goal, or to maximize some related measure of data utility. Over the past decades, two main types of sophisticated DW analysis frameworks have been proposed to identify the most informative monitoring strategy in hydrology, namely, one type based on sensitivity analysis (Dausman et al., 2010; Fienen et al., 2010; Hill and  
85 Tiedeman, 2006) and the other within a fully Bayesian framework (Dai et al., 2016; Neuman et al., 2012; Nowak et al., 2012). The former approaches are computationally fast, but these methods require model calibration and assume linear models (Finsterle, 2015). The latter methods are derived based on the law of the total possibility, without assumptions of the model and of the distributions of observations and model parameters. Nevertheless, both well-established frameworks are predicated on  
90 the availability of the underlying physical models. For example, Man et al. (2016) evaluated the



expected value of alternative SWC sampling strategies with respect to the estimation of soil hydraulic parameters in the Hydrus-1D model, while Finsterle (2015) examined the worth of datasets potentially applicable for the calibration of geothermal reservoir models. Within such parametric data-worth analysis frameworks, however, the strong nonlinearity of soil water problems (De Lannoy et al., 2006; 95 Leube et al., 2012; Yeh et al., 1985) and the prevalence of model structural errors (Zhang et al., 2019) are highly likely to lead to biased data worth (Wang et al., 2018; Wang et al., 2020). Ultimately the reliability of optimal design of monitoring networks based on such evaluations is greatly compromised.

Fortunately, the superiority of data-driven algorithms in handling nonlinearities and structural errors in unsaturated flow has been well demonstrated in our previous studies (Wang et al., 2021a; Wang et al., 2021b). With the explosive growth of big data, how to evaluate the worth of multi-source data in 100 this new data mining approach is becoming a critical issue. Several recent works in the field of statistical learning have bloomed in identifying and removing irrelevant and redundant information from big data, such as feature selection (Chandrashekar and Sahin, 2014; Hall, 1999) and instance reduction (Al-Akhras et al., 2021; Olvera-López et al., 2010). To the best of our knowledge, few 105 studies have systematically evaluated the worth of future observations regarding the construction of fully data-driven models prior to data gathering. As a follow-up study of Wang et al. (2018) and Wang et al. (2020), one major contribution of this study is the first embedding of a purely data-driven model into the Bayesian data-worth analysis framework, referring to as the nonparametric data-worth analysis (NP-DWA). Similar to traditional DW analysis, the proposed NP-DWA consists of prior, posterior, and 110 preposterior stages (Dai et al., 2016). The preposterior analysis evaluates the anticipated worth of future observations regarding the construction of purely data-driven models, for which possible distributions are predicted in advance by conditioning on prior data.

There is a consensus in the field of statistics that “the highest accuracy results that an inductive learning system can achieve depend on the quality of data and on the appropriate selection of a learning 115 algorithm for the data” (Pechenizkiy et al., 2006). In other words, once the algorithm specified, the significance of data noise on learning accuracy as almost the only factor should not be overlooked. Considering the powerful ability of dealing with observational noises of the ensemble Kalman filter (EnKF) (Hamilton et al., 2017; Li et al., 2018), another innovation of this study is the introduction of EnKF into our NP-DWA framework. In conventional DW analysis, the worth of data is primarily 120 embodied in its ability to be utilized or calibrated to adjust physical parameters (Dai et al., 2016;



Finsterle, 2015; Man et al., 2016). In the proposed NP-DWA, nevertheless, future observations are first used to construct data-driven models in the forecast step and then sequentially assimilated with the Kalman update in the analysis step. Ultimately, its combined capacity to reduce system uncertainties in these two ways is defined as its worth. Furthermore, as a typical sequential DA scheme, the EnKF  
125 facilitates the dynamic models as well as its hyperparameters to be updated in real time, so the data utility to modeling system can be detected instantaneously. Eventually, the sampling scheme can be dynamically adjusted to save the monitoring and analysis costs.

Most previous studies are based on synthetic cases, and data-worth analysis in the context of dynamically evolving soil moisture profiles was still poorly studied in a real-world case. For nonlinear  
130 problems, nevertheless, the estimation variance and more sophisticated measures of data utility depend on the actual values of measurements, which are still unknown prior to collection (Leube et al., 2012). It will be more convincing to investigate the data worth regarding the reconstruction of fully data-driven models under real-world cases for unsaturated flow. With the aid of observed data retrieved from three typical stations with different climate regimes, we aim to shed light on the following  
135 questions: (1) as opposed to the traditional way of utilizing data (to calibrate physical parameters), is the worth of observations capable of being accurately quantified by NP-DWA in this new, purely data-driven approach? (2) Given multiple prediction objectives, how does the DW (in the form of various indices) evolve under different hydrometeorological conditions in the determination of fully data-driven soil moisture dynamics? (3) How does the proposed NP-DWA respond to the presence of  
140 multiple levels of data noise? It is strived that this study can provide guidance in the design of future monitoring strategies within the fully data-driven soil water flow models for real-world problems.

The remainder of this paper is organized as follows: Sect. 2 first summarizes the experimental data and methods. Thereinto, the principles of Bayesian DW analysis, nonparametric DA, and the hybrid framework are detailed. Sect. 3 presents the results, and a discussion is contained in Sect. 4. Finally,  
145 conclusions are outlined in Sect. 5.

## 2 Methodology

In Wang et al. (2021a), a nonparametric sequential data assimilation scheme (Kalman-GP) has been proposed based on the filtering equations of EnKF and data-driven modeling with GP. On top of that, this paper further develops a nonparametric data-worth analysis framework to assess the potential  
150 worth of future observations in the reconstruction of dynamical soil water flow models prior to data



collection. Considering that the Kalman-GP have been described in detail in Wang et al. (2021a), only a brief introduction to it is presented here.

## 2.1 Construction of GP Dynamic Models

We aim to determine a Gaussian stochastic process to approximate the relationship between input data  $\mathbf{x}$  and state variable of interest  $y$ . It should be noted that input  $\mathbf{x}$  may consist of any relevant information in addition to the time and location of quantity of interest. As defined in Rasmussen (2003) and Williams and Rasmussen (2006), a GP  $G(\mathbf{x})$  can be fully specified by a mean function  $\mu(\mathbf{x})$  and covariance function  $k(\mathbf{x}, \mathbf{x}')$ , i.e.,  $G(\mathbf{x}) \sim N(\mu(\mathbf{x}), k(\mathbf{x}, \mathbf{x}'))$ . In this study, a linear mean function and an anisotropic squared exponent covariance function are specified (Zhang et al., 2019) as:

$$\mu(\mathbf{x}) = \boldsymbol{\beta}^T \mathbf{x} \quad (1)$$

$$k(\mathbf{x}, \mathbf{x}') = \sigma^2 \exp \left[ - \sum_{l=1}^d \frac{(x_l - x'_l)^2}{\tau_l^2} \right] \quad (2)$$

where  $\boldsymbol{\beta}$  is vector containing  $d$  linear coefficients, i.e.,  $\boldsymbol{\beta} = \{\beta_1, \beta_2, \dots, \beta_d\}$ ;  $d$  is the dimension of  $\mathbf{x}$ ;  $\sigma^2$  controls the marginal variance in the output; and  $\tau_1, \tau_2, \dots, \tau_d$  determine the dependence strength in each of the component directions of  $\mathbf{x}$ .

Next, let  $\mathbf{X} = \{\mathbf{x}^i\}_{i=1}^N$  denote the input of  $N$  training datasets, while the corresponding output can be represented as  $\mathbf{y} = (y^1, y^2, \dots, y^N)^T$ . Then, the hyperparameters of the GP,  $\boldsymbol{\theta} = \{\boldsymbol{\beta}, \sigma^2, \boldsymbol{\tau}\}$ , can be inferred from the training datasets  $\{\mathbf{X}, \mathbf{y}\}$  via log marginal likelihood maximization:

$$L = \log p(\mathbf{y}|\mathbf{X}, \boldsymbol{\theta}) = -\frac{1}{2}(\mathbf{y} - \boldsymbol{\mu})^T \boldsymbol{\Sigma}^{-1}(\mathbf{y} - \boldsymbol{\mu}) - \frac{1}{2} \log |\boldsymbol{\Sigma}| - \frac{n}{2} \log 2\pi \quad (3)$$

where  $\boldsymbol{\mu}$  denotes the prior mean vector, and  $\boldsymbol{\Sigma}$  denotes the covariance matrix whose elements in the  $i$ th row and  $j$ th column constitute  $\Sigma_{ij} = k(\mathbf{x}_i, \mathbf{x}_j)$ . The GPML MATLAB toolbox (version 4.2), as documented in Williams and Rasmussen (2006), was adopted for GP inference in this study (<http://www.gaussianprocess.org/gpml/code/matlab/doc/>).

Finally, the posterior mean  $\mathbf{y}^*$  can be predicted for any new input  $\mathbf{X}^*$  as:

$$\mathbf{y}^* = \boldsymbol{\mu}^* + \boldsymbol{\Sigma}^{*T} \boldsymbol{\Sigma}^{-1}(\mathbf{y} - \boldsymbol{\mu}) \quad (4)$$

where  $\boldsymbol{\mu}^*$  denotes the prior mean of  $\mu(\mathbf{X}^*)$  and  $\boldsymbol{\Sigma}^*$  is calculated as  $\Sigma_i^* = k(\mathbf{x}_i, \mathbf{X}_j^*)$ .

## 2.2 The Kalman Update in Nonparametric Data Assimilation Scheme

Similar to the conventional EnKF method (Evensen, 2003), the model-free DA strategy also comprises forecast and analysis steps. At the forecast step at  $t=k$ ,  $N_1$  GP dynamic models are



175 constructed in the light of  $\{(\mathbf{X}_{1:k-1}, \mathbf{y}_{1:k-1})_1, \dots, (\mathbf{X}_{1:k-1}, \mathbf{y}_{1:k-1})_i, \dots, (\mathbf{X}_{1:k-1}, \mathbf{y}_{1:k-1})_{N_1}\}$   
 independently via Eqs. 1-3. Here,  $(\mathbf{X}_{1:k-1}, \mathbf{y}_{1:k-1})$  represents all available data points from  $t=1$  to  $(k-1)$   
 and  $i$  is the ensemble member index. Hence an ensemble of  $\mathbf{y}^*$  at the current time step,  $\mathbf{Y}_k^f$ , can be  
 forecasted via Eq. 4, which can be expressed as:

$$\mathbf{Y}_k^f = [\mathbf{y}_{k,1}^*, \mathbf{y}_{k,2}^*, \dots, \mathbf{y}_{k,i}^*, \dots, \mathbf{y}_{k,N_1}^*]^T \quad (5)$$

where superscripts  $f$  refers to forecast;  $\mathbf{y}_{k,i}^*$  represents the forecasted state vector of interest for the  $i$ th  
 180 GP model that was constructed at  $t=k$ .

In the analysis step of the EnKF, the resultant forecasted state vector at  $t=k$ ,  $\mathbf{Y}_k^f$ , is updated via the  
 assimilation of current observation data,  $\mathbf{d}_k^{obs}$ :

$$\mathbf{Y}_k^a = \mathbf{Y}_k^f + \mathbf{K}_k(\mathbf{d}_k^{obs} - \mathbf{H}\mathbf{Y}_k^f) \quad (6)$$

where  $\mathbf{Y}_k^a$  denotes the posterior estimates for the ensemble of state vectors conditional on the observed  
 data at  $t=k$ ; superscript  $a$  indicates analysis; and  $\mathbf{H}$  is the observation operator, which represents the  
 185 relationship between the state and observation vectors.

The Kalman gain at  $t=k$ ,  $\mathbf{K}_k$ , can be defined as:

$$\mathbf{K}_k = \mathbf{C}_k^f \mathbf{H}^T (\mathbf{H} \mathbf{C}_k^f \mathbf{H}^T + \mathbf{R}_k)^{-1} \quad (7)$$

where  $\mathbf{R}_k$  is the error covariance matrix of the observations; and  $\mathbf{C}_k^f$  is the covariance matrix of the  
 state vector at  $t=k$ , which can be approximated as:

$$\mathbf{C}_k^f \approx \frac{1}{N_e - 1} \sum_{i=1}^{N_1} \{[\mathbf{y}_{k,i}^f - \langle \mathbf{Y}_k^f \rangle][\mathbf{y}_{k,i}^f - \langle \mathbf{Y}_k^f \rangle]^T\} \quad (8)$$

where  $\mathbf{y}_{k,i}^f$  is equivalent to  $\mathbf{y}_{k,i}^*$  and  $\langle \mathbf{Y}_k^f \rangle$  denotes the ensemble mean of  $\mathbf{Y}_k^f$ .

## 190 2.3 Nonparametric Data-worth Analysis Framework

Following the methodologies of Neuman et al. (2012) and Dai et al. (2016), data-worth analysis of  
 future monitoring networks within the aforementioned NP-DWA framework also consists of three  
 stages. The whole workflow of the NP-DWA framework is depicted in Fig. 1.

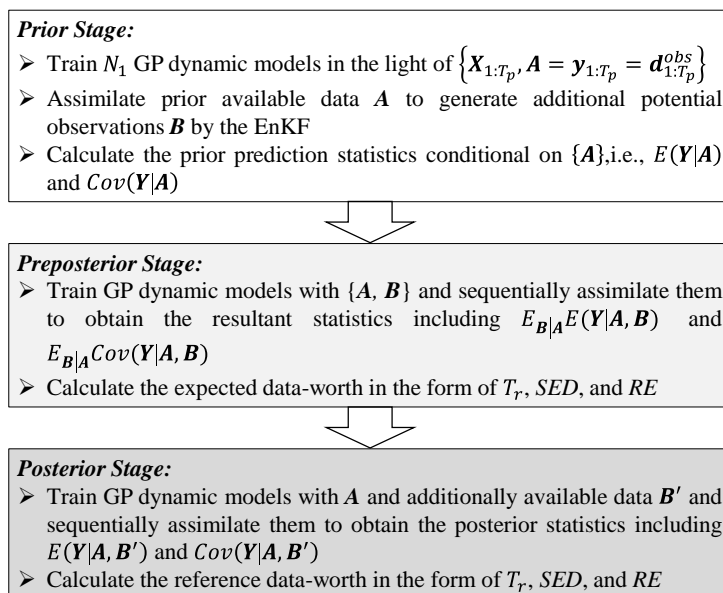
### 2.3.1 Prior Stage

195 At the prior stage ( $0 < t \leq T_p$ ), the integration of GP dynamic models and EnKF with an ensemble  
 size of  $N_1$  is implemented to sequentially train and assimilate the prior data via Eqs. 1–8. Here, all  
 available prior datasets from  $t=0$  to  $t=T_p$  are denoted as  $\mathbf{A} = \mathbf{y}_{1:T_p} = \mathbf{d}_{1:T_p}^{obs}$ , while the corresponding  
 GP input is denoted as  $\mathbf{X}_{1:T_p}$ . Then, a set of  $N_e$  hypothetical observations can be generated, denoted as



$\mathbf{B}_{k,i} = \mathbf{H}_k \mathbf{y}_{k,i}^f$  ( $k = T_p + 1, T_p + 2, \dots, T_t$ ;  $i = 1, 2, \dots, N_1$ ), via Eq. 4.  $T_t$  is the total simulation time.

200 Moreover, prior prediction statistics (mean and covariance) of posterior vector  $\mathbf{Y}_k$ , i.e.,  $E(\mathbf{Y}|\mathbf{A})$  and  $Cov(\mathbf{Y}|\mathbf{A})$ , can be yielded conditional on  $\{\mathbf{A}\}$ , which can be denoted as  $\mathbf{E}_1$  and  $\mathbf{C}_1$ , respectively, for the sake of simplicity.



205 **Figure 1.** The workflow of nonparametric data-worth analysis framework coupled with Ensemble Kalman Filter (EnKF)

### 2.3.2 Preposterior Stage

At the preposterior stage ( $T_p + 1 < t \leq T_t$ ), for each possible data  $\mathbf{B}_{k,i}$  at  $t=k$ ,  $N_2$  realizations satisfying a Gaussian distribution are further generated. The ensemble mean is the value of  $\mathbf{B}_{k,i}$ , while the variance is the measurement error. Since this method is recursive, the time index  $k$  is omitted in the following equations. Then, the integration of GP models and EnKF is again implemented through a set of  $N_2$  Monte Carlo realizations for each of the  $N_1$  hypothetical observations. This allows us to calculate prediction statistics of the posterior state vector  $\mathbf{Y}_{ij}$  ( $i = 1, 2, \dots, N_1$ ;  $j = 1, 2, \dots, N_2$ ), i.e.,  $E(\mathbf{Y}_i|\mathbf{A}, \mathbf{B}_i)$  and  $Cov(\mathbf{Y}_i|\mathbf{A}, \mathbf{B}_i)$ , conditional on  $\{\mathbf{A}, \mathbf{B}_i\}$ . Finally, quantities  $E_{\mathbf{B}|\mathbf{A}}E(\mathbf{Y}|\mathbf{A}, \mathbf{B})$ ,  $E_{\mathbf{B}|\mathbf{A}}Cov(\mathbf{Y}|\mathbf{A}, \mathbf{B})$ , and  $Cov_{\mathbf{B}|\mathbf{A}}E(\mathbf{Y}|\mathbf{A}, \mathbf{B})$  can be yielded by averaging over the collection of  $N_1 \times N_2$  realizations. It should be emphasized that  $E_{\mathbf{B}|\mathbf{A}}E(\mathbf{Y}|\mathbf{A}, \mathbf{B})$  and  $E_{\mathbf{B}|\mathbf{A}}Cov(\mathbf{Y}|\mathbf{A}, \mathbf{B})$  represent the preposterior prediction mean and uncertainty after the addition of future possible data  $\mathbf{B}$ , which can be





denoted as  $\mathbf{E}_2$  and  $\mathbf{C}_2$ , respectively.

To quantify the expected data-worth of potential measurements, three commonly considered information metrics, including the trace ( $T_r$ ), Shannon entropy difference ( $SED$ ), and relative entropy ( $RE$ ), are introduced in this study.  $T_r$  and  $SED$  offer scalar indices to measure the decrease in variance and covariance, respectively, while the  $RE$  comprehensively quantifies both mean and covariance effects.

(1) Trace

As a scalar indicator (Dai et al., 2016),  $T_r$  quantifies the DW in terms of variance reduction as follows:

$$T_r = T_r(\mathbf{C}_1) - T_r(\mathbf{C}_2) \quad (9)$$

where  $T_r(*)$  denotes the trace (sum of the diagonal entries) of a matrix.

(2) Shannon entropy difference

According to Shannon (1949), the Shannon entropy ( $SE$ ) of PDF  $p(x)$  can be defined as:

$$SE(p) = - \int p(x) \ln p(x) dx, x \in R \quad (10)$$

The  $SED$  between the prior and posterior PDFs can also be considered to quantify the information content extracted from additional observations. Assuming that these two PDFs are both Gaussian in the EnKF model, the  $SED$  can be expressed in terms of covariance reduction (Xu, 2007) as:

$$SED = \frac{\ln \det(\mathbf{C}_1)}{2} - \frac{\ln \det(\mathbf{C}_2)}{2} = \frac{\ln \det(\mathbf{C}_1 \mathbf{C}_2^{-1})}{2} \quad (11)$$

where  $\det(*)$  is the determinant of a matrix.

(3) Relative entropy

Similar to the  $SED$ , the  $RE$  also provides a measure of the information content of the posterior PDF with respect to the prior PDF. In addition to uncertainty reduction, the influence of future data on the mean behavior of PDFs is considered (Singh et al., 2013; Zhang et al., 2015). Considering that the prior and posterior PDFs are  $n$ -dimensional Gaussian functions, the  $RE$  can be defined as:

$$RE = \frac{1}{2}(\mathbf{E}_2 - \mathbf{E}_1)^T \mathbf{C}_1^{-1}(\mathbf{E}_2 - \mathbf{E}_1) + \frac{1}{2}[\ln \det(\mathbf{C}_1 \mathbf{C}_2^{-1}) + T_r(\mathbf{C}_2 \mathbf{C}_1^{-1}) - n] \quad (12)$$

Finally, the expected DW of  $\mathbf{B}_k$  can be estimated in the form of the above three indices prior to data gathering. Similar procedures are repeated until the final time  $t=T_t$  is reached.

### 2.3.3 Posterior Stage

At the posterior stage ( $T_p + 1 < t \leq T_t$ ), the available actual dataset  $\mathbf{B}'$  is incorporated into the GP



training datasets and assimilated in a sequential manner. The actual mean and covariance of posterior state vector  $Y$ , i.e.,  $E(Y|A, B')$  and  $Cov(Y|A, B')$ , respectively, are obtained conditional on  $\{A, B'\}$ .  
245 The reference data-worth in the form of the various indices can be calculated via Eqs. 9–12, where  $E_2$  and  $C_2$  are replaced with  $E(Y|A, B')$  and  $Cov(Y|A, B')$ , respectively.

### 3 Description of experimental data and model setup

#### 3.1 Data Sources and Site Description

Three typical sites, including Falkenberg (52.1669 N, 14.1241 E), Cape\_Charles\_5\_ENE (37.2907 N,  
250 75.9270 W, hereafter referred to as Cape), and DAHRA (15.4035 N, 15.4320 W) were selected from the International Soil Moisture Network (ISMN, <https://ismn.geo.tuwien.ac.at/en/>) to evaluate the performance of the proposed NP-DWA framework under different soil types and climatic regimes. According to the dominant fraction of clay, silt, and sand for two layers (topsoil: 0.0–0.3 m, subsoil: 0.3–1.0 m) provided by ISMN, we use the USDA soil texture classification and classified the soil at  
255 three sites. The soil at Falkenberg is sandy loam, and the DAHRA soil is loamy sand. The topsoil and subsoil at Cape are clay loam and loamy clay, respectively. At these three sites, the in situ volumetric SWC was operationally measured with TRIME-EZ (IMKO), Stevens Hydraprobe II Sdi-12 (Stevens Water Inc.), and ThetaProbe ML2X (Delta-T Devices) instruments, respectively. The measurement depths were (1) 0.08, 0.15, 0.30, 0.45, 0.60, and 0.90 m at the Falkenberg site, (2) 0.05, 0.10, 0.20, 0.50,  
260 and 1.00 m at the Cape site, and (3) 0.05, 0.10, 0.50, and 1.00 m at the DAHRA site. The measurement error was assumed to be  $0.02 \text{ cm}^3/\text{cm}^3$  unless otherwise specified.

Apart from soil water measurements at different depths, the daily precipitation and air temperature at the height of 2 meters were obtained from the ISMN. At each site, 200-day time series (from January 15 and August 2 in 2005 at the Falkenberg site, from April 24 to November 9 in 2004 at the Cape site,  
265 and from April 9 to October 25 in 2011 at the DAHRA site) were collected in this study, as shown in Fig. 2. Having a continental climate, the Falkenberg receives frequent but less intense precipitation during the simulation period. The Cape has a humid subtropical climate with the highest rates rainfall among the three sites, and there were a few rainstorm events during the study period (e.g., up to 150 mm/d on September 8, 2014). The region of DAHRA has a tropical climate with well-defined dry and  
270 humid seasons. The early stage of the simulation is in its dry season, with little to no rainfall. The late stage is in its humid season when frequent but less intense rainfall events occurs and the daily average air temperature is about  $30 \text{ }^\circ\text{C}$ .

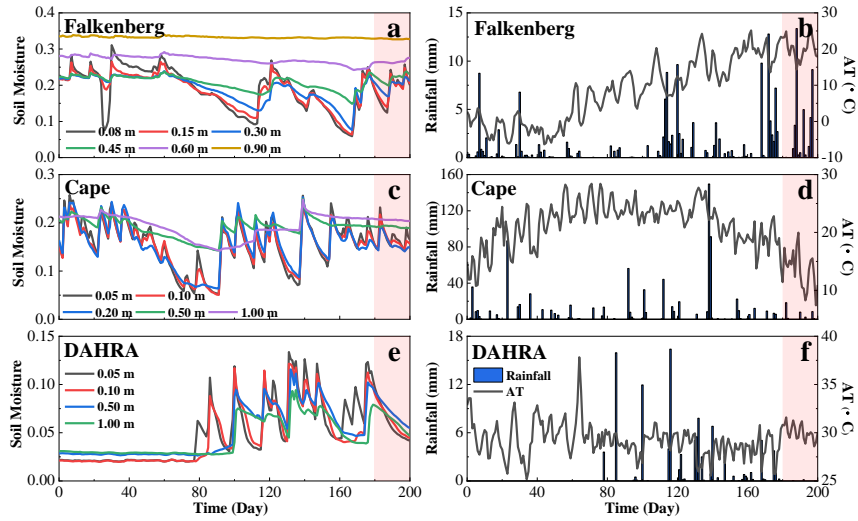


**Figure 2.** The temporal evolutions of soil moisture at various depths, daily rainfall, and mean daily air temperature (AT) at 2 meters height at Falkenberg, Cape, and DAHRA, respectively. Note that the red area indicates the preposterior or posterior stage

### 3.2 Model Simulation Setup and Case Design

The key parameters of this study are summarized in Table 1. Each site is represented by a one-dimensional soil column with a height of 1 m, which is discretized into 2cm grids with local refinement of 1-cm monitoring depth intervals, i.e.,  $z=0.15$  m and 0.45 m at the Falkenberg site and  $z=0.05$  m at the Cape and DAHRA sites. At each time step,  $N_1 = 50$  GP-based dynamic models of unsaturated flow are constructed. The GP model input  $x$  includes the observation time, depth, daily precipitation, and air temperature, while the output is the corresponding soil moisture. The state vector  $y$  comprises the soil moisture for all nodes at each site, and the trained and assimilated observations  $d^{obs}$  refer to the available soil moisture at all observed depths (as described in Sect. 3.1).

We illustrate our approach based on a set of real-world test cases, as listed in Table 2. The performance of the three indices, namely,  $T_r$ ,  $SED$ , and  $RE$ , in data-worth quantification are compared at all three sites. In this study, the worth of potential observations regarding the retrieval of three quantities of interest (QoI), including  $\theta_{1.00}^{ave}$ ,  $\theta_{0.60}^{ave}$ , and  $\theta_{0.30}^{ave}$ , is evaluated. Here,  $\theta_{1.00}^{ave}$ ,  $\theta_{0.60}^{ave}$ , and  $\theta_{0.30}^{ave}$  represent the average soil moisture in the top 1.00 m, 0.60 m, and 0.30 m, respectively. A comparison among cases TC1, TC2, and TC3, is designed to investigate the data-worth response of surface ( $\theta_s$ ),



middle ( $\theta_M$ ), and deep ( $\theta_D$ ) SWC regarding the above different prediction objectives. The prior datasets entering these cases comprise of SWC at various depths, daily precipitation, and air temperature over 295 the first 80 days, as shown in the gray areas of Fig. 2. The subsequent 20-day data (red areas in Fig. 2) are augmented as additional data for reference DW assessment in the posterior stage.

**Table 1.** The summary of key parameters

Parameter	Value
Description of soil column	
Soil column height [m]	1.00
No. of Nodes	53 (Falkenberg)/52 (Cape&DAHRA)
Number of realizations	
$N_1$	50
$N_2$	50
Prior values of GP hyperparameters	
$\tau_1, \tau_2, \tau_3, \tau_4$	1
$\sigma^2$	0.5
$\beta_1, \beta_2, \beta_3, \beta_4$	0

**Table 2.** The summary of designed test cases and main characteristics

Case Name	Potential Observation	Observation Error	Prior Data (d)	Variable of Interest
TC1	TC1-1 $\theta_S$	0.02 <sup>2</sup>	80	$\theta_{1.00}^{ave}$
	TC1-2 $\theta_M$	0.02 <sup>2</sup>	80	$\theta_{1.00}^{ave}$
	TC1-3 $\theta_D$	0.02 <sup>2</sup>	80	$\theta_{1.00}^{ave}$
TC2	TC2-1 $\theta_S$	0.02 <sup>2</sup>	80	$\theta_{0.60}^{ave}$
	TC2-2 $\theta_M$	0.02 <sup>2</sup>	80	$\theta_{0.60}^{ave}$
	TC2-3 $\theta_D$	0.02 <sup>2</sup>	80	$\theta_{0.60}^{ave}$
TC3	TC3-1 $\theta_S$	0.02 <sup>2</sup>	80	$\theta_{0.30}^{ave}$
	TC3-2 $\theta_M$	0.02 <sup>2</sup>	80	$\theta_{0.30}^{ave}$
	TC3-3 $\theta_D$	0.02 <sup>2</sup>	80	$\theta_{0.30}^{ave}$
TC4	$\theta_S$	0.01 <sup>2</sup>	80	$\theta_{1.00}^{ave}$
TC5	$\theta_S$	0.04 <sup>2</sup>	80	$\theta_{1.00}^{ave}$
TC6	$\theta_S$	0.02 <sup>2</sup>	40	$\theta_{1.00}^{ave}$
TC7	$\theta_S$	0.02 <sup>2</sup>	180	$\theta_{1.00}^{ave}$
TC8	$\theta_S, \theta_M$	0.02 <sup>2</sup>	80	$\theta_{1.00}^{ave}$
TC9	$\theta_S, \theta_M, \theta_D$	0.02 <sup>2</sup>	80	$\theta_{1.00}^{ave}$



Notes:  $\theta_S$ ,  $\theta_M$ , and  $\theta_D$  refer to soil moisture in the surface, middle, and deep layers, respectively;  $\theta_{1,00}^{ave}$ ,  $\theta_{0,60}^{ave}$ , and  $\theta_{0,30}^{ave}$  refer to average soil moisture in the top 1.00 m, 0.60 m, and 0.30 m, respectively.

As stated in Pechenizkiy et al. (2006) and Zhu and Wu (2004), the maximum accuracy of statistical learning algorithms mainly depends on the quality of training data, in addition to the inherent bias in the algorithm itself. In other words, the magnitude and accuracy of the expected worth of driving data in machine learning-based DA may be closely related to the noise level. Thus, two additional test cases (TC4 and TC5) are considered to evaluate the performance of the proposed NP-DWA framework under different measurement errors. The soil moisture measurement error variance values of  $0.01^2$  and  $0.04^2$  are assumed in TC4 and TC5, respectively, to be compared to a value of  $0.02^2$  in TC1-1.

Moreover, test cases TC6 and TC7 differ from test case TC1-1. These test cases are designed to investigate the influence of the prior data content on data-worth analysis, which facilitates the determination of the required prior information content to ensure the accuracy of data-worth assessment. The 80-day prior data in test case TC1-1 are reduced backward in time to 40 days in test case TC6 and augmented forward to 180 days in test case TC7. In addition, test cases TC1-1, TC8, and TC9 consider the composite DW of different combinations of monitoring schemes. The comprehensive contributions of the surface SWC jointly with the middle and/or deep ones are compared with its individual contribution.

### 3.3 Evaluation setup

To compare the relative differences in data-worth estimation accuracy under the various test scenarios, the mean absolute percentage error (MAPE) between the expected and reference data-worth in the form of  $T_r$ ,  $SED$ , and  $RE$  is defined as:

$$MAPE = \frac{1}{T_t - T_p} \sum_{k=T_p+1}^{T_t} \left| \frac{DW_k^{Expect} - DW_k^{Refer}}{DW_k^{Refer}} \right| \quad (13)$$

where  $DW_k^{Expect}$  and  $DW_k^{Refer}$  denote the expected and reference DW values, respectively, at time step  $t=k$ .

## 4 Results and discussions

### 4.1 Optimal Monitoring Location for the Multiple Predictive Objectives (TC1/TC2/TC3)

Fig. 3 shows the probability distributions of the generated potential observation realizations as well as their ensemble mean and the corresponding actual observations of the surface ( $\theta_S$ ), middle ( $\theta_M$ ), and



deep ( $\theta_D$ ) soil moisture at three sites. Only the results on the 81<sup>st</sup>, 90<sup>th</sup>, and 99<sup>th</sup> days are presented here. Overall, the  $N_1 = 50$  potential realizations could “capture” the actual SWC observations with acceptable accuracy. Specifically, the forecasted middle SWC exhibited a considerably more robust ‘capturing’ performance with sustained better proximity of potential and actual  $\theta_M$  throughout the simulation period. This occurred especially pronounced at the Cape site. For example, both surface and deep layers at Cape may be at risk of poor fit of potential observations to measurements (Fig. 3d and Fig. 3w), while the generated middle SWC is always fairly well approximated to the corresponding actual values in Fig. 3(m-o).

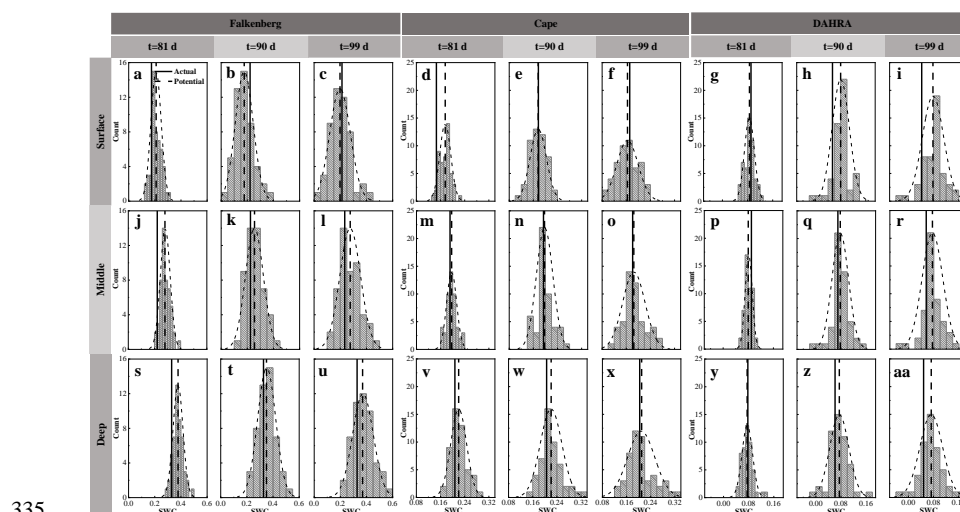


**Figure 3.** The probability distributions (dotted curved line) of potential observation realizations as well as their mean (dotted vertical line) and the corresponding actual soil water content (SWC) observation (solid line) in the surface, middle, and deep layers on the 81<sup>st</sup>, 90<sup>th</sup>, and 99<sup>th</sup> day at Falkenberg, Cape, and DAHRA, respectively

Based on the above potential observations, their expected data-worth regarding the retrieval of  $\theta_{1.00}^{ave}$ ,  $\theta_{0.60}^{ave}$ , and  $\theta_{0.30}^{ave}$  can be quantified in the form of  $T_r$ ,  $SED$ , and  $RE$ , as depicted in Fig. 4. Meanwhile, for ease of analysis, Fig. 5 compares the covariance matrixes of entire soil moisture profile in the prior stage, preposterior stage, and posterior stage. Only the results from the 81<sup>st</sup> day to 90<sup>th</sup> day at Falkenberg are revealed here. It can be observed that despite an overall increasing trend over time, the values of expected DW were prone to local spikes due to changes in the atmospheric boundary conditions such as rainfall. First of all, this general trend of increase should be attributed to the



sequential augmentation of potential observations based on existing prior data, resulting in the cumulative values of DW over time. However, abrupt changes in external forcing, such as unexperienced rainfall events on the 88<sup>th</sup> day at the Falkenberg, could trigger temporal extrapolation of statistical learning (Li et al., 2020; Minns and Hall, 1996; Xu and Valocchi, 2015), which in turn led to a surge in prior predictive uncertainty, i.e.,  $C_1 = Cov(Y|A)$  (the 1<sup>st</sup> column of Fig. 5). Fortunately, joint GP training and sequential assimilation of real-time potential observations can effectively lower the risk of such irrational extrapolation (Wang et al., 2021a; Wang et al., 2021b), allowing these temporal mutations to be substantially attenuated at the preposterior stage [i.e.,  $C_2 = E_{B|A}Cov(Y|A, B)$ ] (the 2<sup>nd</sup>-4<sup>th</sup> column of Fig. 5). This uncertainty reduction brought about by the fusion of additional data became significantly larger when external forcing encountered mutations, which ultimately led to the localized surge in DW during rainfall events.

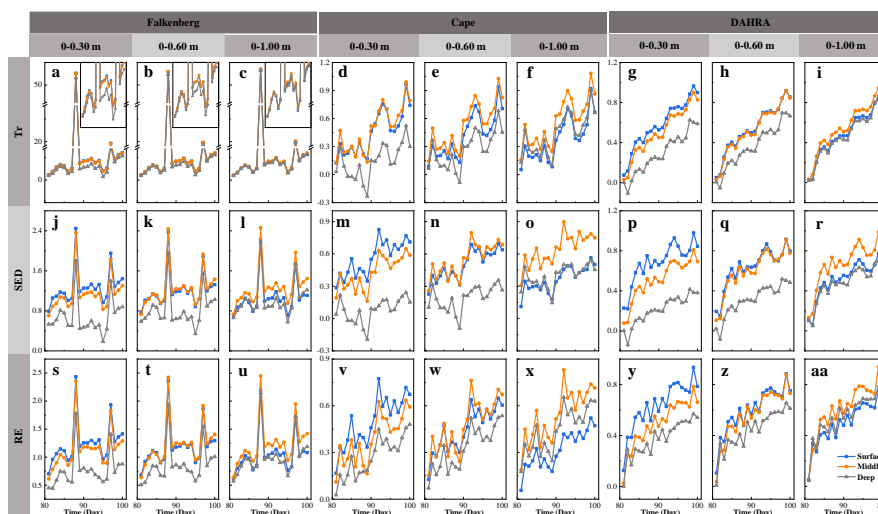


**Figure 4.** The expected data-worth of potential soil moisture observations in the surface, middle, and deep layers in the form of trace ( $T_r$ ), Shannon entropy difference ( $SED$ ), and relative entropy ( $RE$ ), respectively, regarding the retrieval of average soil moisture in the top 0.30 m, 0.60 m, and 1.00 m at three sites

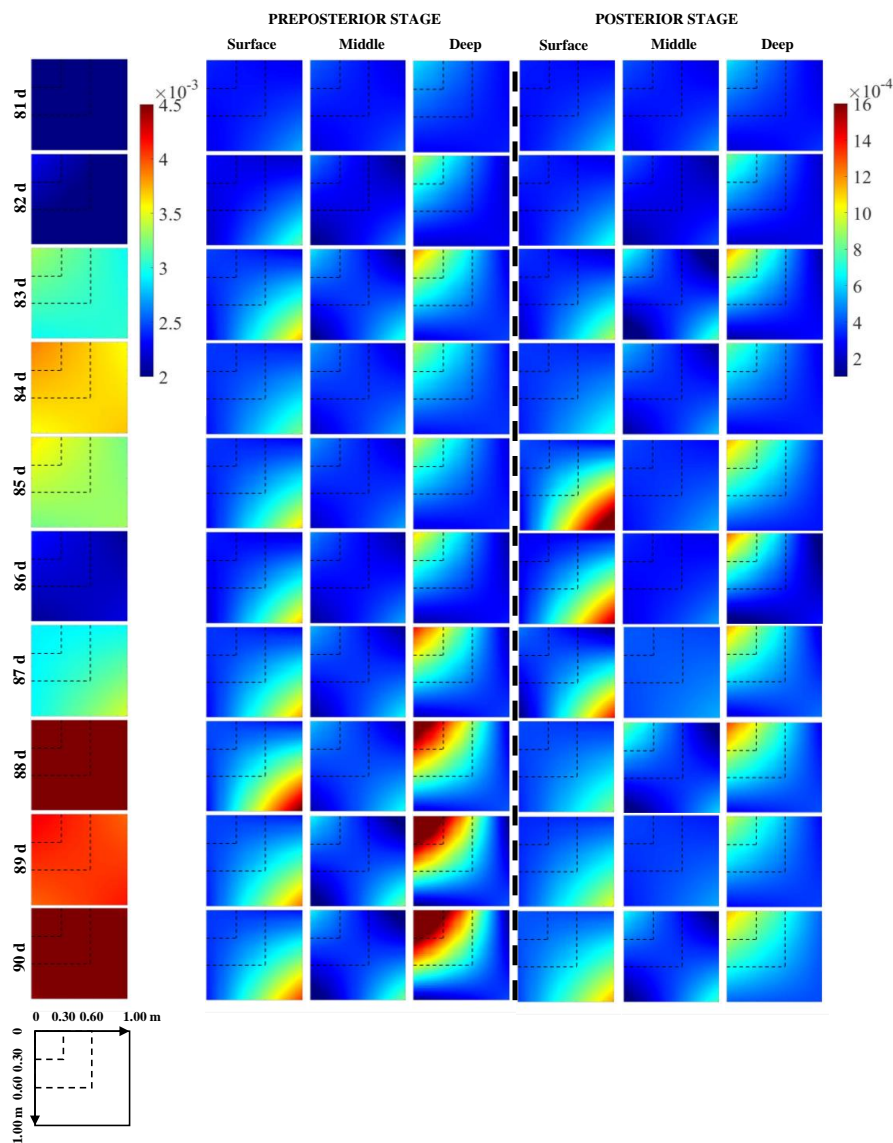


**Figure 5.** The covariance matrixes of soil moisture profiles from the 81<sup>st</sup> to 90<sup>th</sup> day at Falkenberg before (column 1) and after potential (columns 2-4) and corresponding actual (columns 5-7) soil moisture observations in the surface, middle, and deep layers were fused, respectively

Moreover, Fig. 4 also suggests that the optimal observation depth shifted as the prediction target changed. As expected, the surface SWC  $\theta_s$  produced higher  $T_r$ ,  $SED$ , and  $RE$  values regarding the estimation of  $\theta_{0,30}^{ave}$ . As the depth range of the average SWC to be estimated was extended downward,



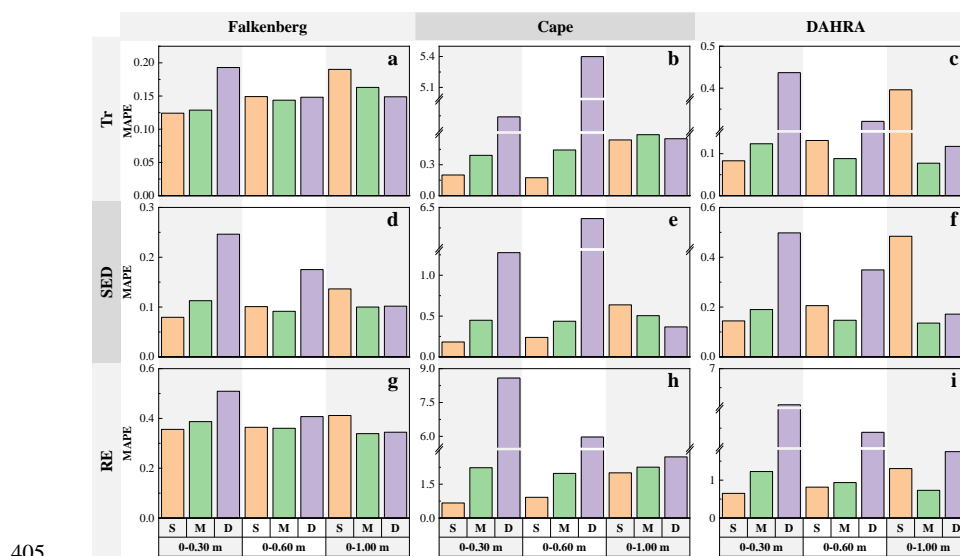


370 the data-worth advantages of  $\theta_M$  and  $\theta_D$  began to emerge. Surprisingly, the potential middle SWC  
still exhibited a considerably higher superiority even in  $\theta_{1.00}^{ave}$  estimation. In other words, the soil  
moisture in the middle layer has the most robust advantage in data-worth. This may be due to the fact  
that the integration of surface or deep SWC only reduced the uncertainty within the corresponding  
depth ranges (the 2<sup>nd</sup> and 4<sup>th</sup> column of Fig. 5), whereas the augmentation of  $\theta_M$  significantly decrease  
375 the covariance matrixes of the entire SWC profiles (the 3<sup>rd</sup> column of Fig. 5). This selection result of  
the optimal monitoring location seemingly contradicts previous findings within the traditional  
parametric DW analysis where the surface observations with the largest temporal variation always  
produced the greatest data worth, as reported in Dai et al. (2016) and Wang et al. (2018). This  
discrepancy is likely to depend on the different mechanisms that characterize soil moisture dynamics in  
380 the vertical direction between the two approaches. The traditional parametric unsaturated flow model  
follows the law of mass conservation-based physical governing equations (i.e., the  
Richardson–Richards equation, (Richards, 1931; Richardson, 1922)). The strongest time-varying nature  
of surface SWC was conducive to effective updating of the physical parameters in EnKF, eventually  
generating the maximum data-worth (Wang et al., 2018). However, the spatial prediction performance  
385 of data-driven methods substantially hinged on the similarity of data between different depths.  
Theoretically, there occurs an inherent delayed response of soil moisture profiles to rainfall events,  
which has been well-documented experimentally (Wierenga et al., 1986; Bresler et al., 1971; Vauclin et  
al., 1979). This causes the temporal changes in surface and deep SWC to be naturally asynchronous,  
thus rendering their representativeness in characterizing the whole soil moisture profile somewhat  
390 limited. Ultimately, the complete reliance on statistical and information-theoretic measures allowed the  
most representative middle SWC to establish the most robust superiority in DW.

It can also be seen from Fig.4 that when using different information indices (i.e.,  $T_r$ ,  $SED$ , and  $RE$ )  
to quantify the data-worth, the optimal observation location selected is identical, regardless of soil  
textures and climatic regimes. This conclusion is generally in line with Wang et al. (2018) and Man et  
395 al. (2016). Furthermore, to quantify the data-worth assessment accuracy, Fig. 6 depicts the MAPE  
between the expected and reference data-worth in the form of  $T_r$ ,  $SED$ , and  $RE$  of alternative  
monitoring schemes at the different depths. It can be observed that the surface SWC yielded the  
smallest MAPE when retrieving  $\theta_{0.30}^{ave}$ , regardless of the metric type. During the estimation of  $\theta_{0.60}^{ave}$   
and  $\theta_{1.00}^{ave}$ , nevertheless, the expected data-worth of  $\theta_M$  more accurately and robustly approached the



400 reference counterparts with overall smaller MAPEs. We recall that this ranking of DW estimation accuracy was exactly in line with the ranking of the magnitude of their expected DW in Fig. 4. To be specific, a comparison of Fig. 4 and Fig. 6 reveals that potential observations with a larger expected DW are prone to a higher DW estimation accuracy due to its more robust ability of “imitating” the actual observations (Fig. 3).



405 **Figure 6.** The MAPEs between expected and reference data-worth in the form of  $T_r$ ,  $SED$ , and  $RE$  of potential soil moisture observations in the surface (S), middle (M), and deep (D) layers, respectively, regarding the retrieval of average soil moisture in the top 0.30 m, 0.60 m, and 1.00 m at three sites

410 **4.2 Effects of Observation Noise (TC1-1/TC4/TC5)**

Fig. 7 shows the probability distributions of the potential observation ensemble as well as their mean and the corresponding actual observations of the surface SWC under different SWC noise levels. Similarly, only the results on the 81<sup>st</sup>, 90<sup>th</sup>, and 99<sup>th</sup> days are displayed. It can be observed that a higher noise level was not always detrimental but rather instead expanded the distribution width along the SWC-axis and produced a flatter curve. The risk of failure of the generated realizations to “capture” the real observations was thus reduced. Even on the 81<sup>st</sup> day at Falkenberg, for example, the increase in SWC error variance from 0.01<sup>2</sup> to 0.04<sup>2</sup> facilitated a better agreement between the potential and actual surface soil moisture, as revealed in Fig. 7 (a j s). Similar phenomena can also be found via a



comparison of Fig. 7e and Fig. 7n.

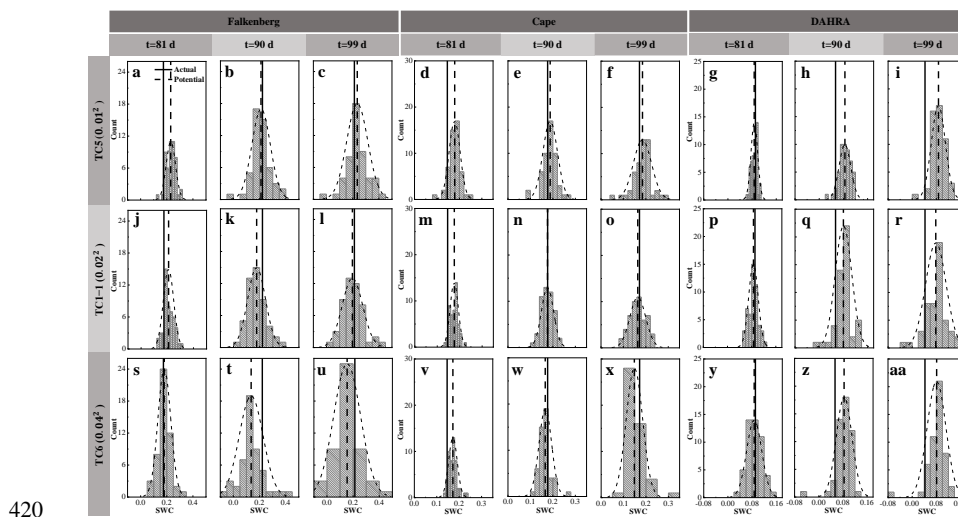


**Figure 7.** The probability distributions (dotted curved line) of potential observation realizations as well as their mean (dotted vertical line) and the corresponding actual soil water content (SWC) observations (solid line) in the surface layer on the 81<sup>st</sup>, 90<sup>th</sup>, and 99<sup>th</sup> day at three sites under different measurement error variances being  $0.01^2$  (TC4),  $0.02^2$  (TC1-1), and  $0.04^2$  (TC5), respectively

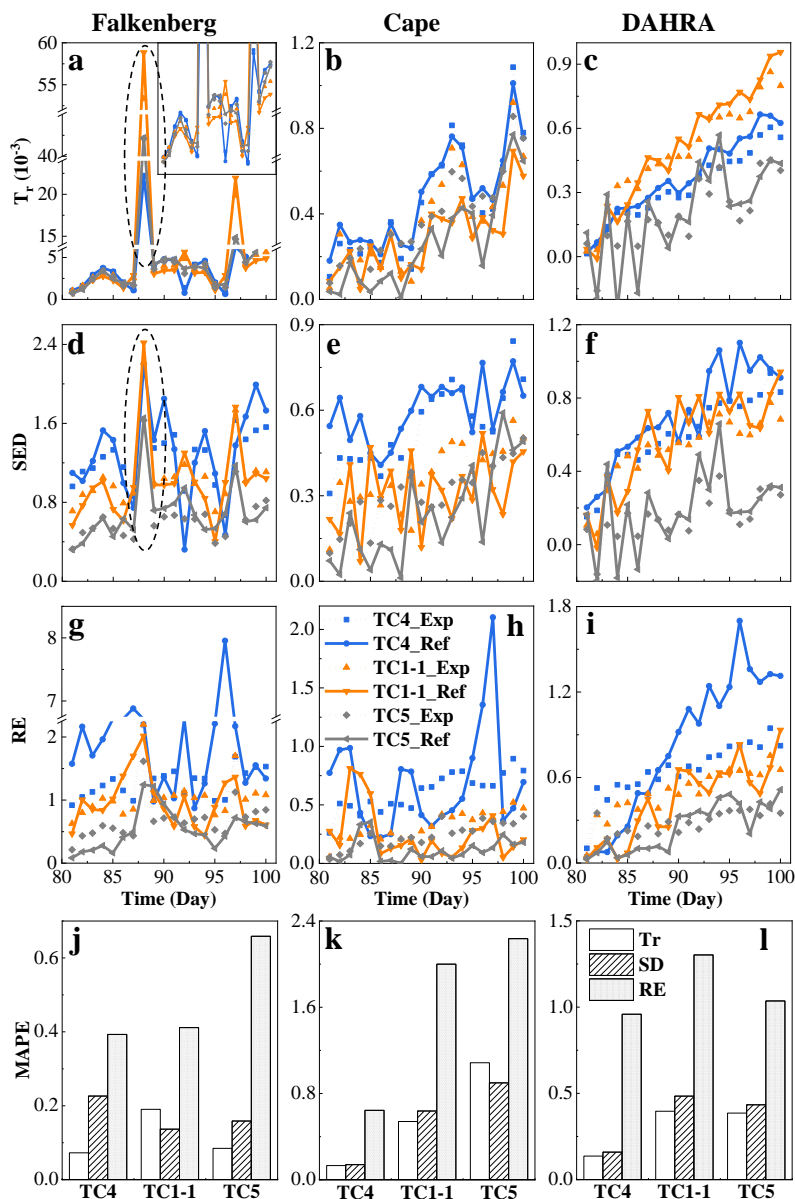
425

Fig. 8 shows the temporal evolution and time-averaged MAPE of the expected and reference data-worth in the form of three information indices, respectively, under various noise levels. Some interesting findings can be obtained: (1) Overall, the potential SWC data corrupted by a lower noise level yielded larger data-worth with higher accuracy. (2) Nevertheless, the occurrence of rainfall events triggered a futile DW increase while also rendering the potential observations with appropriately magnified observation errors more valuable. For instance, a properly inflated observation error of  $0.02^2$  on the 88<sup>th</sup> day at the Falkenberg site resulted in a notably higher data-worth than that of  $0.01^2$ , as highlighted by the dashed ellipse boxes in Fig. 8a and Fig. 8d. Furthermore, this increase in data-worth resulting from noise amplification was particularly evident in the form of  $T_r$  over the other two metrics, as depicted in Fig. 8(a-c) and Fig. 8(d-i). At DAHRA, potential observations with an observation error of  $0.02^2$  even produced a significantly higher  $T_r$  value than that of  $0.01^2$  throughout almost the entire simulation period (Fig. 8c). (3) As opposed to  $T_r$  and  $SED$  indices focusing only on the system uncertainty (variance or covariance), the expected  $RE$ , as a comprehensive mean-covariance-type

435



metric, was often more challenging to approach its reference counterparts with the largest MAPE at all 440 sites, as shown in Fig. 8(j-l).



**Figure 8.** The temporal evolution (a-i) and time-averaged MAPEs (j-l) of the expected and reference data-worth in the form of  $T_r$ ,  $SED$ , and  $RE$  at three sites, respectively, under different measurement error variances being  $0.01^2$  (TC4),  $0.02^2$  (TC1-1), and  $0.04^2$  (TC5), respectively



#### 4.3 Effects of Prior Data Content (TC1-1/TC6/TC7)

Fig. 9(a-i) depicts the temporal evolution of the expected and reference data-worth of the surface SWC in cases TC6, TC1-1, and TC7 with the 40-day, 80-day, and 180-day prior data content, respectively. Under normal circumstances, an increase in the available prior data content inevitably entails a shrinkage in the DW of subsequent data due to the possibility of information redundancy. However, this seems to be valid only for a modest increase in prior data (from 40-day to 80-day) within our NP-DWA framework. The substantial augmentation in available data content from 80-day to 180-day instead resulted in a notably higher DW of the additional data (Fig. 9). Even more unexpectedly, this DW growth was prevalent across sites, regardless of the soil types and climatic regimes. To clarify this anomaly, Fig. 10 further shows the predicted covariance matrixes of soil moisture profiles conditional on  $\{A\}$  in prior stage and  $\{A, B\}$  in preposterior stage in cases TC6, TC1-1, and TC7, respectively. Only the results from the 81<sup>st</sup> day to 90<sup>th</sup> day at Falkenberg are presented here. Our previous studies have demonstrated that although the mean values of potential samples can approach actual observations well in fully (Wang et al., 2021a) or partially (Zhang et al., 2019) data-driven dynamical systems, their ensemble was apt to suffer from considerable uncertainty (Wang et al., 2021b). Unfortunately, augmented prior data, despite its potential to enrich available GP training scenarios, failed to prevent the non-convergence of  $N_e = 50$  GP samples. In contrast, the additional noise associated with prior data supplementation could exacerbate the increase in the prior prediction uncertainty (i.e.,  $C_1$ ), as illustrated by a comparison between the first three columns of Fig. 10. It should be highlighted that the fusion of  $B$  enabled a notable reduction in the preposterior uncertainties (i.e.,  $C_2$ ) in the data assimilation system to a comparable level (the last three columns of Fig. 10), even with different prior data content. The gradual widening of the gap between  $C_1$  and  $C_2$  eventually yielded the highest data-worth with the maximum amount of prior data in test case TC7 (Fig. 9). This seems to alarm us that uncontrolled expansion of big data within fully data-driven systems may not be beneficial. The adverse effects of extra noise may overshadow its original superiority in generalization capability. Access to high-quality and representative “small” data may constitute the key to the successful application of fully data-driven algorithms for reshaping soil moisture dynamics.

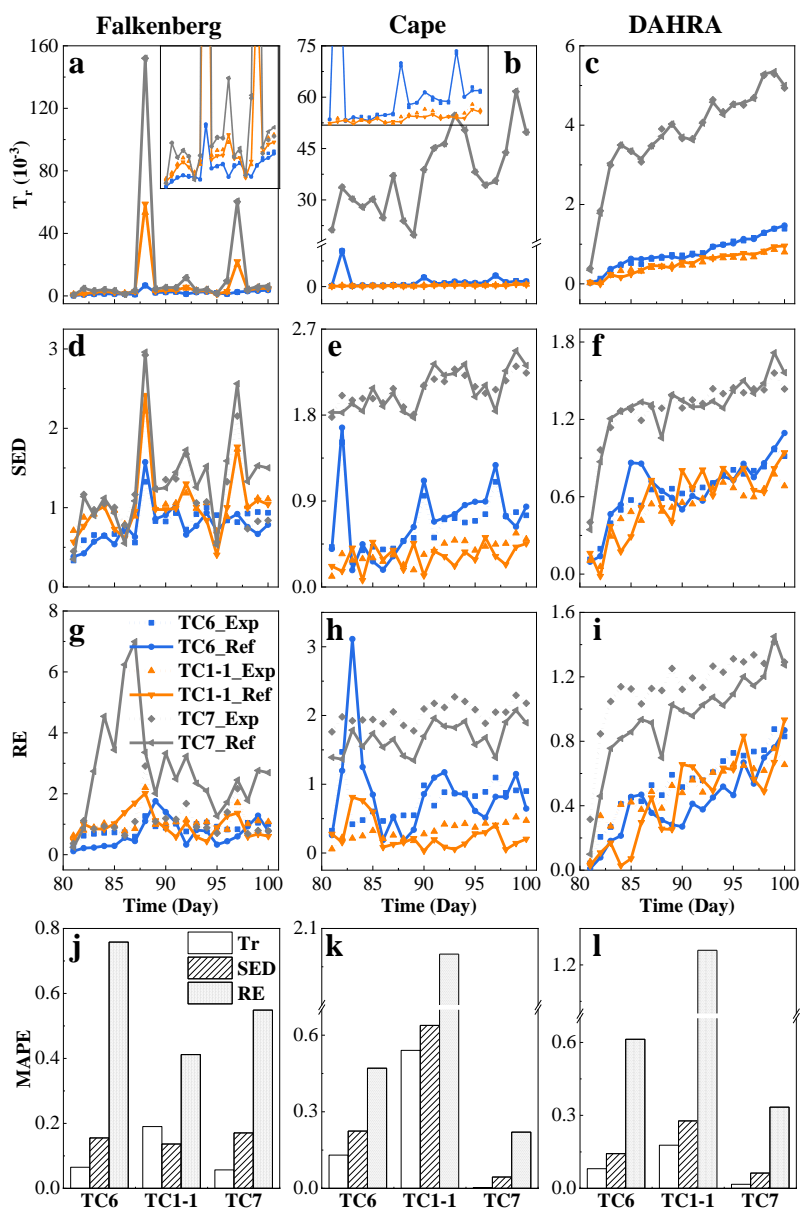


**Figure 9.** The temporal evolution (a-i) and time-averaged MAPEs (j-l) of the expected and reference data-worth in the form of  $T_r$ ,  $SED$ , and  $RE$  at three sites for cases TC6, TC1-1, and TC7 with 40-day, 80-day, and 180-day prior data content, respectively

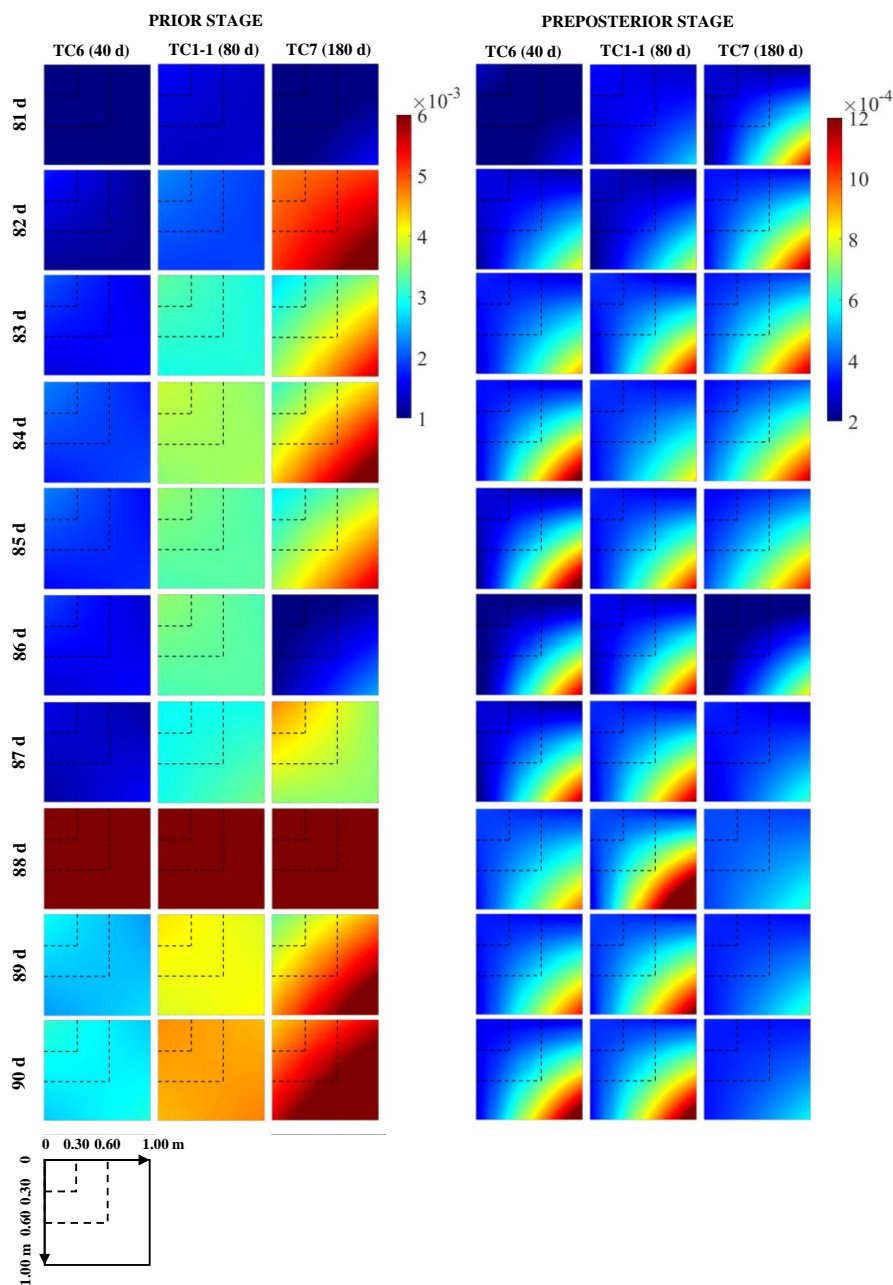


**Figure 10.** The covariance matrixes of soil moisture profiles from the 81<sup>st</sup> day to 90<sup>th</sup> day at Falkenberg in the prior and preposterior stage for cases TC6, TC1-1, and TC7 with 40-day, 80-day, and 180-day prior data content,

480 respectively



Furthermore, Fig. 9(j-l) depicts the time-averaged MAPE in the expected and reference data-worth in cases TC6, TC1-1, and TC7, respectively. A comparison of Fig. 9(a-i) and Fig. 9(j-l) reveals some interesting findings: (1) similar to the results in Sect. 4.1, the potential measurements with the largest expected (or reference) data-worth in TC7 are apt to possess the highest estimation accuracy of data-worth. (2) Local variations in data-worth at different sites respond slightly differently to the augmentation of prior data content. For instance, even with 180 days of available historical data, the DW spike induced by the unexperienced rainfall event on the 88<sup>th</sup> day at the Falkenberg has not been eliminated or diminished (Fig. 9(a d g)). However, similar DW surges on the 82<sup>nd</sup> day at Cape were successfully mitigated as the amount of prior data content increased from 40-day (TC6) to 80-day (TC1-1) (Fig. 9(e h)). This is because the prior data at Falkenberg, even if augmented to 180-day, did not cover the rainfall event on the 88<sup>th</sup> day (Fig. 2b), whereas the 80-day training data at Cape already included the scenario on the 82<sup>nd</sup> (Fig. 2d). These results agree with the conclusions reported in Wang et al. (2020) that the diversity of scenarios in the training data is more decisive than the data volume regarding the performance of data-driven methods. (3) Although inferior to  $T_r$  and  $SED$ , the estimation accuracy of  $RE$  is generally acceptable, especially when prior data is expanded to 180 days. This is certainly a remarkable improvement over the rather poor performance of  $RE$  in traditional parametric data-worth analysis (Wang et al., 2018; Wang et al., 2020). This progress should be attributed to the radical abandonment of physical models in the NP-DWA, which prevented adverse effects of the high nonlinearity of soil water flow in the propagation of uncertainties from input to output (i.e., soil moisture in this study). Direct mapping from regular meteorological data to SWC facilitated the identification of the soil moisture covariance matrix from potential observations.

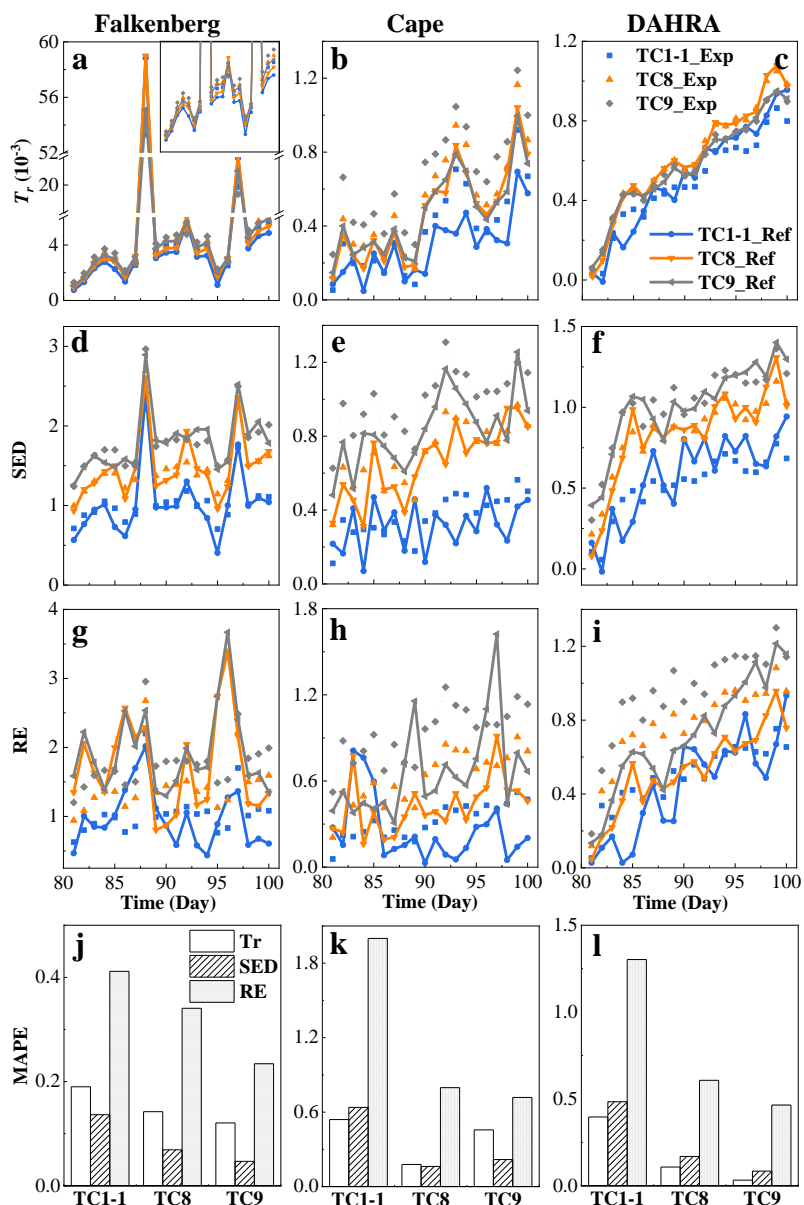
#### 4.4 Effects of potential observational combinations (TC1-1/TC8/TC9)

Fig. 11(a-i) compares the expected (and reference) data-worth of three combinations of potential observations at different depths at the three sites. It can be seen that the composite data-worth of the alternative monitoring schemes exhibited an increasing pattern as the depth range of the observed SWC continues to expand downward. Nevertheless, the response of the different data-worth indicators and study sites to this vertical expansion of potential observations varied slightly. Further integration of  $\theta_D$  in TC9 did not cause a marked increase in  $T_r$ , but yielded notably greater  $SED$  and  $RE$  values, especially at the DAHRA site (Fig. 11(c f d)). This is undoubtedly due to the extra consideration of the latter two indicators for the non-diagonal elements of the covariance matrix or/and the behavior of the mean.





Moreover, the joint fusion of potential  $\theta_S$  and  $\theta_M$  failed to result in a sustained increase in  $T_r$  and  $RE$  at DAHRA, while creating a significant increase in composite DW at the other two sites. This could be attributed to the sandy soil texture at DAHRA (with the fraction of sand up to 90%, and  $K_s=3.22$  m/d),  
 515 resulting in the almost synchronous responses of the SWC at  $z=0.05$  m and  $0.50$  m to the atmospheric boundary conditions (Fig. 2e) and thus triggering possible data redundancy.

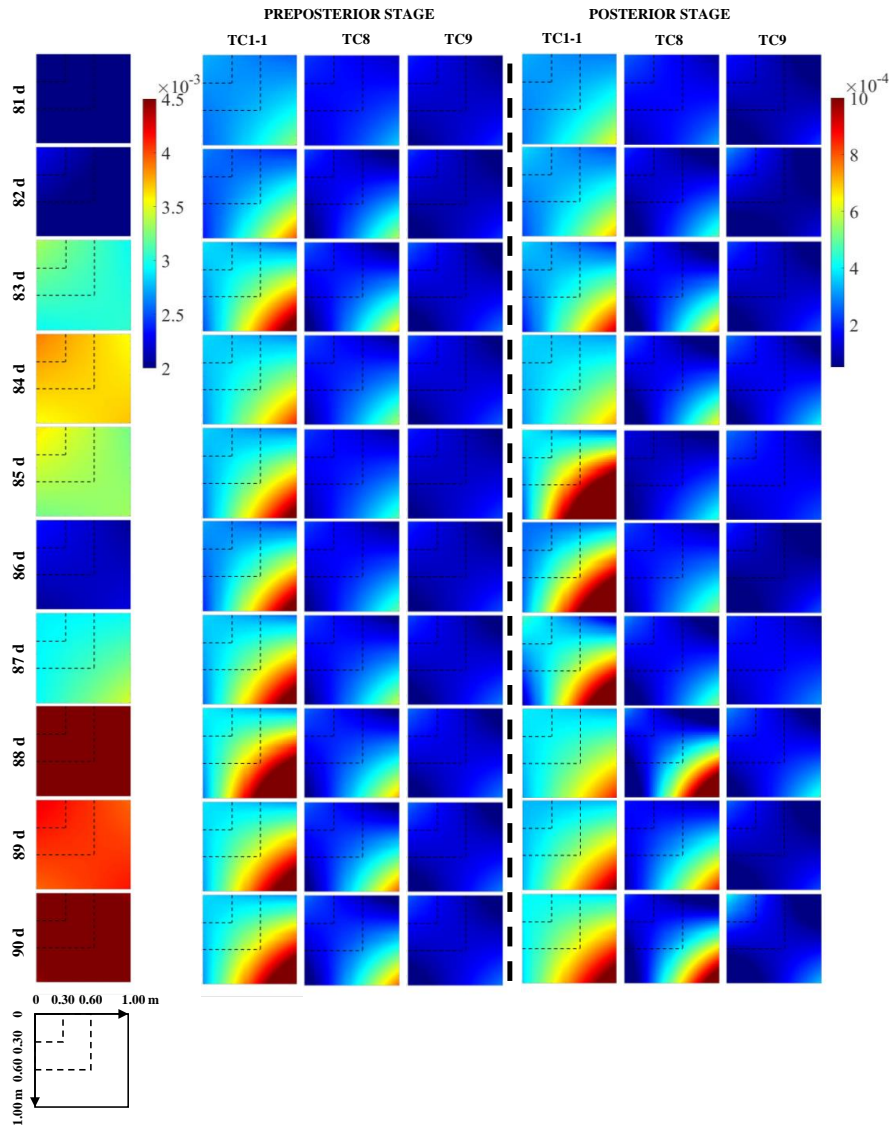


**Figure 11.** The temporal evolution (a-i) and time-averaged MAPEs (j-l) of the expected and reference data-worth



in the form of  $T_r$ ,  $SED$ , and  $RE$  at three sites for cases TC1-1 (surface soil moisture), TC8 (surface & middle soil  
520 moisture), and TC9 (surface & middle & deep soil moisture), respectively

Fig. 11(j-l) further shows the estimation accuracy of expected data-worth for the above three potential observation combinations. Surprisingly, the increase in the number of potential observations, while making it more difficult to “capture” actual SWC data, ends up significantly improving the  
525 accuracy of the data-worth assessment. As shown in Fig. 11(j-l), as more potential observations along the vertical direction were evaluated, the MAPEs between expected data-worth and its reference counterparts decreased continuously. This phenomenon actually breaks the misconceptions about the data-worth assessment accuracy in previous studies, i.e., that an excellent fit of potential observations is equivalent to high-precision estimates of the corresponding data-worth. For the sake of explanation, Fig.  
530 12 shows the predicted covariance matrixes of soil moisture profiles in cases TC1-1, TC8, and TC9 from the 81<sup>st</sup> day to 90<sup>th</sup> day at Falkenberg conditional on  $\{A\}$ ,  $\{A, B\}$ , and  $\{A, B'\}$ , respectively. It can be found that compared to TC1-1, which only reduces the uncertainties in the surface SWC, the integration of observations at multiple depths clearly reduces the uncertainties in the entire SWC profiles to a considerably lower level. This ultimately facilitates better proximity between expected and  
535 reference covariance matrixes, as revealed in the 4<sup>th</sup> and 7<sup>th</sup> columns in Fig. 12. The above results suggest that the accuracy of data-worth assessment of potential observations does not only depend on their capacity to “capture” actual measurements, but is also closely related to their correlation with the variable of interest. We recall that similar phenomena also exist in the preceding test cases. For example, the weaker correlation between surface SWC observations and  $\theta_{1,00}^{avg}$  led to deterioration in  
540 the DW estimation performance with the largest MAPE values (Fig.6(a d g)) even if the actual surface observations could be suitably reproduced (Fig. 3(a-c)). Therefore, to enhance the reliability of data-worth assessment, a strategy wherein potential observations at multiple depths were simultaneously incorporated into existing DA systems was recommended in this study.



545 **Figure 12.** The covariance matrixes of soil moisture profiles from the 81<sup>st</sup> day to 90<sup>th</sup> day at Falkenberg before  
 (column 1) and after potential (columns 2-4) and actual observations (columns 5-7) for cases TC1-1 (surface soil  
 moisture), TC8 (surface & middle soil moisture), and TC9 (surface & middle & deep soil moisture) were fused,  
 respectively

550 **5 Conclusions**

Conventional data-worth analysis for soil water problems depends on physical dynamic models.



Due to the widespread occurrence of model structural errors, it may lead to biased or wrong worth assessment. The strong nonlinearity of unsaturated flow further deteriorates the DW assessment performance in the retrieval of soil moisture profiles. This study proposed a nonparametric data-worth  
555 analysis method within a fully data-driven modeling framework. The information extracted from real-time soil moisture data after GP training and Kalman update was quantified with three representative types of indicators, i.e., variance- ( $T_r$ ), covariance- ( $SED$ ), and mean-covariance-type ( $RE$ ) indicators. With the aid of a series of real-world cases, the ability and challenge of the NP-DWA in terms of the variables of interest, spatial location, observation error, and prior data content were  
560 assessed. The following conclusions were drawn:

(1) The proposed NP-DWA framework enabled an accurate assessment of the data-worth of potential observations regarding the reconstruction of purely data-driven soil water flow models prior to data collection. Nevertheless, the overall increasing trend of the DW from the sequential augmentation of additional observations was susceptible to interruptions by localized surges due to  
565 never-experienced atmospheric conditions within the NP-DWA framework. Fortunately, the adverse effects of anomalous GP extrapolation in our nonparametric approach could be suitably avoided by the enrichment of training scenarios in prior data. Moreover, the appropriate amplification of observational noise under extreme meteorological conditions also facilitated the alleviation of this biased estimates by enhancing the generalization capacity of dynamic models.

(2) The optimal observation depth shifted as the prediction target varied. In contrast to the notably  
570 higher DW of surface SWC observations within the conventional DW analysis framework, middle SWC observations tended to exhibit considerably higher robustness in the construction of model-free soil moisture dynamic models. This should be attributed to the ability of the SWC in the middle layer to effectively reduce the predictive uncertainty of the entire soil moisture profiles due to its optimal representativeness. The inherent delayed response of soil moisture profiles to rainfall events allowed  
575 this advantage of middle SWC prevalent across sites, even becoming increasingly pronounced with increasing delay effect.

(3) Although the addition of prior data content could greatly improve the estimation accuracy of the expected DW, the ensuing observation noise could substantially increase the uncertainty in a purely  
580 data-driven DA system, leading to potentially higher data-worth of subsequent observations. Hence, high-quality and representative small data may be regarded as a better choice than unfiltered big data.



(4) An alternative monitoring strategy with a larger data-worth was prone to a higher DW assessment accuracy within the proposed NP-DWA framework. Specifically, the performance of data-worth assessment was jointly determined by ‘3Cs’, i.e., capacity of potential observation  
585 realizations to “capture” actual observations, correlation of potential observations with the predicted variables of interest, and choice of DW quantitative indicators. Furthermore, the direct mapping from regular meteorological data to SWC in our nonparametric method facilitated the identification of the soil moisture covariance matrix (especially the cross-covariance) due to its alleviation of highly nonlinearity of soil water flow problems. Hence, satisfactory estimation accuracy could also be  
590 achieved even with covariance-related data-worth metrics (i.e., the *SED* and *RE*).

#### ACKNOWLEDGEMENTS

This work was supported by the National Natural Science Foundation of China Grants U2243235 and 51979200, and the Open Research Fund of Guangxi Key Laboratory of Water Engineering  
595 Materials and Structures Grant GXHRI-WEMS-2020-06.

#### CODE/DATA AVAILABILITY

The code/data that support the findings of this study are available from the corresponding author upon reasonable request.

#### 600 AUTHOR CONTRIBUTION

**Yakun Wang:** Conceptualization, Methodology, Software, Writing–original draft. **Xiaolong Hu:** Conceptualization, Software. **Lijun Wang:** Methodology. **Jinmin Li:** Data curation, Methodology. **Lin Lin:** Supervision. **Kai Huang:** Data curation. **Liangsheng Shi:** Writing – review & editing, Supervision.  
605

#### COMPETING INTERESTS

The contact author has declared that none of the authors has any competing interests.

#### References:

610 Akhtar, K. et al., 2019. Wheat straw mulching offset soil moisture deficient for improving physiological and growth performance of summer sown soybean. *Agricultural water management*,



- 211: 16-25.
- Al-Akhras, M., El Hindi, K., Habib, M. and Shawar, B.A., 2021. Instance reduction for avoiding overfitting in decision trees. *Journal of Intelligent Systems*, 30(1): 438-459.
- 615 Brajard, J., Carrassi, A., Bocquet, M. and Bertino, L., 2020. Combining data assimilation and machine learning to emulate a dynamical model from sparse and noisy observations: A case study with the Lorenz 96 model. *Journal of Computational Science*, 44: 101171.
- Brajard, J., Carrassi, A., Bocquet, M. and Bertino, L., 2021. Combining data assimilation and machine learning to infer unresolved scale parametrization. *Philosophical Transactions of the Royal Society A*, 379(2194): 20200086.
- 620 A, 379(2194): 20200086.
- Bresler, E. et al., 1971. Infiltration from a trickle source: II. Experimental data and theoretical predictions. *Soil Science Society of America Journal*, 35(5): 683-689.
- Chandrashekar, G. and Sahin, F., 2014. A survey on feature selection methods. *Computers & Electrical Engineering*, 40(1): 16-28.
- 625 Dai, C., Xue, L., Zhang, D. and Guadagnini, A., 2016. Data-worth analysis through probabilistic collocation-based Ensemble Kalman Filter. *Journal of Hydrology*, 540: 488-503.
- Dausman, A.M., Doherty, J., Langevin, C.D. and Sukop, M.C., 2010. Quantifying data worth toward reducing predictive uncertainty. *Groundwater*, 48(5): 729-740.
- De Lannoy, G.J., Verhoest, N.E., Houser, P.R., Gish, T.J. and Van Meirvenne, M., 2006. Spatial and temporal characteristics of soil moisture in an intensively monitored agricultural field (OPE3). *Journal of Hydrology*, 331(3-4): 719-730.
- 630 Journal of Hydrology, 331(3-4): 719-730.
- Dobriyal, P., Qureshi, A., Badola, R. and Hussain, S.A., 2012. A review of the methods available for estimating soil moisture and its implications for water resource management. *Journal of Hydrology*, 458: 110-117.
- 635 Dunne, S. and Entekhabi, D., 2005. An ensemble - based reanalysis approach to land data assimilation. *Water resources research*, 41(2).
- Evensen, G., 2003. The ensemble Kalman filter: Theoretical formulation and practical implementation. *Ocean dynamics*, 53(4): 343-367.
- Fielen, M.N., Doherty, J.E., Hunt, R.J. and Reeves, H.W., 2010. Using prediction uncertainty analysis to design hydrologic monitoring networks: example applications from the Great Lakes water availability pilot project. U. S. Geological Survey.
- 640 to design hydrologic monitoring networks: example applications from the Great Lakes water availability pilot project. U. S. Geological Survey.



- Finsterle, S., 2015. Practical notes on local data - worth analysis. *Water Resources Research*, 51(12): 9904-9924.
- García, S., Ramírez-Gallego, S., Luengo, J., Benítez, J.M. and Herrera, F., 2016. Big data  
645 preprocessing: methods and prospects. *Big Data Analytics*, 1(1): 1-22.
- García-Gil, D., Luengo, J., García, S. and Herrera, F., 2019. Enabling smart data: noise filtering in big data classification. *Information Sciences*, 479: 135-152.
- Gu, H., Lin, Z., Guo, W. and Deb, S., 2021. Retrieving surface soil water content using a soil texture adjusted vegetation index and unmanned aerial system images. *Remote Sensing*, 13(1): 145.
- 650 Hall, M.A., 1999. Correlation-based feature selection for machine learning. The University of Waikato. Hamilton, F., Berry, T. and Sauer, T., 2017. Kalman-Takens filtering in the presence of dynamical noise. *The European Physical Journal Special Topics*, 226(15): 3239-3250.
- Hill, M.C. and Tiedeman, C.R., 2006. Effective groundwater model calibration: with analysis of data, sensitivities, predictions, and uncertainty. John Wiley & Sons.
- 655 Hughes, G., 1968. On the mean accuracy of statistical pattern recognizers. *IEEE transactions on information theory*, 14(1): 55-63.
- Ju, L., Zhang, J., Meng, L., Wu, L. and Zeng, L., 2018. An adaptive Gaussian process-based iterative ensemble smoother for data assimilation. *Advances in water resources*, 115: 125-135.
- Kashif Gill, M., Kemblowski, M.W. and McKee, M., 2007. Soil moisture data assimilation using  
660 support vector machines and ensemble Kalman filter 1. *JAWRA Journal of the American Water Resources Association*, 43(4): 1004-1015.
- Kisekka, I., Migliaccio, K.W., Muñoz Carpena, R., Schaffer, B. and Khare, Y., 2015. Modelling soil water dynamics considering measurement uncertainty. *Hydrological Processes*, 29(5): 692-711.
- Leube, P.C., Geiges, A. and Nowak, W., 2012. Bayesian assessment of the expected data impact on  
665 prediction confidence in optimal sampling design. *Water Resources Research*, 48(2).
- Li, C. and Ren, L., 2011. Estimation of unsaturated soil hydraulic parameters using the ensemble Kalman filter. *Vadose Zone Journal*, 10(4): 1205-1227.
- Li, P. et al., 2020. Comparison of the use of a physical-based model with data assimilation and machine learning methods for simulating soil water dynamics. *Journal of Hydrology*, 584: 124692.
- 670 Li, X., Shi, L., Zha, Y., Wang, Y. and Hu, S., 2018. Data assimilation of soil water flow by considering multiple uncertainty sources and spatial - temporal features: a field-scale real case study. *Stochastic*



- Environmental Research and Risk Assessment, 32(9): 2477-2493.
- Liu, H.L. et al., 2011. Simulating water content, crop yield and nitrate-N loss under free and controlled tile drainage with subsurface irrigation using the DSSAT model. *Agricultural Water Management*, 675 98(6): 1105-1111.
- Liu, K. et al., 2020. A gaussian process-based iterative Ensemble Kalman Filter for parameter estimation of unsaturated flow. *Journal of Hydrology*, 589: 125210.
- Man, J., Zhang, J., Li, W., Zeng, L. and Wu, L., 2016. Sequential ensemble - based optimal design for parameter estimation. *Water Resources Research*, 52(10): 7577-7592.
- 680 Metzger, J.C. et al., 2017. Vegetation impacts soil water content patterns by shaping canopy water fluxes and soil properties. *Hydrological processes*, 31(22): 3783-3795.
- Minns, A.W. and Hall, M.J., 1996. Artificial neural networks as rainfall-runoff models. *Hydrological sciences journal*, 41(3): 399-417.
- Montzka, C. et al., 2011. Hydraulic parameter estimation by remotely-sensed top soil moisture 685 observations with the particle filter. *Journal of hydrology*, 399(3-4): 410-421.
- Neuman, S.P., Xue, L., Ye, M. and Lu, D., 2012. Bayesian analysis of data-worth considering model and parameter uncertainties. *Advances in Water Resources*, 36: 75-85.
- Nowak, W., Rubin, Y. and de Barros, F.P., 2012. A hypothesis - driven approach to optimize field campaigns. *Water Resources Research*, 48(6).
- 690 Olvera-López, J.A., Carrasco-Ochoa, J.A., Martínez-Trinidad, J. and Kittler, J., 2010. A review of instance selection methods. *Artificial Intelligence Review*, 34(2): 133-143.
- Pechenizkiy, M., Tsymbal, A., Puuronen, S. and Pechenizkiy, O., 2006. Class noise and supervised learning in medical domains: The effect of feature extraction. *IEEE*, pp. 708-713.
- Rasmussen, C.E., 2003. *Gaussian processes in machine learning*. Springer, pp. 63-71.
- 695 Reichle, R.H., Crow, W.T. and Keppenne, C.L., 2008. An adaptive ensemble Kalman filter for soil moisture data assimilation. *Water resources research*, 44(3).
- Renard, K.G., 1997. *Predicting soil erosion by water: a guide to conservation planning with the Revised Universal Soil Loss Equation (RUSLE)*. United States Government Printing.
- Richards, L.A., 1931. Capillary conduction of liquids through porous mediums. *Physics*, 1(5): 318-333.
- 700 Richardson, L.F., 1922. *Weather prediction by numerical process*. University Press.
- Ross, P.J., 2003. *Modeling soil water and solute transport—Fast, simplified numerical solutions*.





- Agronomy journal, 95(6): 1352-1361.
- Shannon, C.E., 1949. Communication in the presence of noise. *Proceedings of the IRE*, 37(1): 10-21.
- Shi, C., Xie, Z., Qian, H., Liang, M. and Yang, X., 2011. China land soil moisture EnKF data  
705 assimilation based on satellite remote sensing data. *Science China Earth Sciences*, 54(9): 1430-1440.
- Shuwen, Z., Haorui, L., Weidong, Z., Chongjian, Q. and Xin, L.I., 2005. Estimating the soil moisture  
profile by assimilating near-surface observations with the ensemble Kalman filter (EnKF). *Advances  
in Atmospheric Sciences*, 22(6): 936-945.
- Šimůnek, J., Van Genuchten, M.T. and Šejna, M., 2006. The HYDRUS software package for  
710 simulating two-and three-dimensional movement of water, heat, and multiple solutes in  
variably-saturated media. Technical manual, version, 1: 241.
- Singh, K., Sandu, A., Jardak, M., Bowman, K.W. and Lee, M., 2013. A practical method to estimate  
information content in the context of 4D-Var data assimilation. *SIAM/ASA Journal on Uncertainty  
Quantification*, 1(1): 106-138.
- 715 Song, X., Shi, L., Ye, M., Yang, J. and Navon, I.M., 2014. Numerical comparison of iterative ensemble  
Kalman filters for unsaturated flow inverse modeling. *Vadose Zone Journal*, 13(2): 1-12.
- Van Dam, J.C. and Feddes, R.A., 2000. Numerical simulation of infiltration, evaporation and shallow  
groundwater levels with the Richards equation. *Journal of Hydrology*, 233(1-4): 72-85.
- Van Genuchten, M.T., 1980. A closed - form equation for predicting the hydraulic conductivity of  
720 unsaturated soils. *Soil science society of America journal*, 44(5): 892-898.
- Vauclin, M., Khanji, D. and Vachaud, G., 1979. Experimental and numerical study of a transient, two  
- dimensional unsaturated - saturated water table recharge problem. *Water Resources Research*,  
15(5): 1089-1101.
- Wang, Y. et al., 2018. Sequential data-worth analysis coupled with ensemble Kalman filter for soil  
725 water flow: A real-world case study. *Journal of Hydrology*, 564: 76-88.
- Wang, Y. et al., 2020. A robust data - worth analysis framework for soil moisture flow by hybridizing  
sequential data assimilation and machine learning. *Vadose Zone Journal*, 19(1): e20026.
- Wang, Y. et al., 2021a. A nonparametric sequential data assimilation scheme for soil moisture flow.  
*Journal of Hydrology*, 593: 125865.
- 730 Wang, Y., Shi, L., Zhang, Q. and Qiao, H., 2021b. A gradient-enhanced sequential nonparametric data  
assimilation framework for soil moisture flow. *Journal of Hydrology*, 603: 126857.



- Wierenga, P.J., Gelhar, L.W., Simmons, C.S., Gee, G.W. and Nicholson, T.J., 1986. Validation of stochastic flow and transport models for unsaturated soils: A comprehensive field study. Pacific Northwest Lab., Richland, WA (USA); New Mexico State Univ., Las ...
- 735 Williams, C.K. and Rasmussen, C.E., 2006. Gaussian processes for machine learning, 2. MIT press Cambridge, MA.
- Xu, Q., 2007. Measuring information content from observations for data assimilation: Relative entropy versus Shannon entropy difference. *Tellus A: Dynamic Meteorology and Oceanography*, 59(2): 198-209.
- 740 Xu, T. and Valocchi, A.J., 2015. Data-driven methods to improve baseflow prediction of a regional groundwater model. *Computers & Geosciences*, 85: 124-136.
- Yamanaka, A., Maeda, Y. and Sasaki, K., 2019. Ensemble Kalman filter-based data assimilation for three-dimensional multi-phase-field model: Estimation of anisotropic grain boundary properties. *Materials & Design*, 165: 107577.
- 745 Yang, J., Li, B. and Shiping, L., 2000. A large weighing lysimeter for evapotranspiration and soil - water - groundwater exchange studies. *Hydrological processes*, 14(10): 1887-1897.
- Yeh, T.C.J., Gelhar, L.W. and Gutjahr, A.L., 1985. Stochastic analysis of unsaturated flow in heterogeneous soils: 1. Statistically isotropic media. *Water Resources Research*, 21(4): 447-456.
- Zha, Y. et al., 2019. Review of numerical solution of Richardson - Richards equation for variably saturated flow in soils. *Wiley Interdisciplinary Reviews: Water*, 6(5): e1364.
- 750 Zha, Y., Shi, L., Ye, M. and Yang, J., 2013. A generalized Ross method for two-and three-dimensional variably saturated flow. *Advances in Water Resources*, 54: 67-77.
- Zhang, J., Zeng, L., Chen, C., Chen, D. and Wu, L., 2015. Efficient Bayesian experimental design for contaminant source identification. *Water Resources Research*, 51(1): 576-598.
- 755 Zhang, Q. et al., 2019. A dynamic data-driven method for dealing with model structural error in soil moisture data assimilation. *Advances in Water Resources*, 132: 103407.
- Zhu, X. and Wu, X., 2004. Class noise vs. attribute noise: A quantitative study. *Artificial intelligence review*, 22(3): 177-210.